ISSN: 2754-4966

Journal of Nanosciences Research & Reports

SCIENTIFIC Research and Community

Research Article

Open Access

Effects of Ag Doping Concentrations on Structural and Optical Properties of Citrus Reticulata Capped ZnO Nanoparticles

Joan Jepngetich*, Peter W Njoroge, Sylvia Opiyo and Sharon Kiprotich

Department of Physical and Biological Sciences, Murang'a University of Technology, PO BOX 75, Murang'a 10200, Kenya

ABSTRACT

Dopants are used to modify the properties of metal oxides. They are classified into p type and ntype. The p type dopants are electron acceptors and they reduce the bandgap energy. The n- type dopants are electron donors. Ag+ have two characteristics features such that they can be used in place of substitution and interstitial. Citrus reticulata capped silver doped zinc oxide nanoparticles (AgZnONPs) were synthesized via chemical precipitation method, with Citrus reticulata acting as capping, reducing and stabilizing agents. The nanoparticles were synthesized at different doping concentrations of silver (Agx-ZnO) (x=0.1, 0.25, 0.5, 0.75, 1.0, 1.5, and 2.0 %). The effects of different dopant concentration on structural and optical properties of Citrus reticulata capped ZnO nanoparticles were investigated using X-ray diffraction (XRD), Ultra Violet- Visible spectrophotometer (UV-Vis), Fourier transform Infrared spectroscopy (FT-IR) and Photoluminescence (PL) spectroscopy. The XRD pattern obtained showed that hexagonal wurzite structure of ZnO nanoparticles was retained on addition of Ag as a dopant. 0.1% Ag-ZnO displayed highest peak in XRD pattern at plane [101]. The crystal size of the nanoparticles ranged from 15.2919.87nm. At 0.5% Ag-ZnONPs, the XRD peak shifted to higher 2 theta degrees compared to other doping concentrations. The bandgap energies of Ag-ZnONPs were estimated using Tauc's plot. The bandgap energies were observed to decrease with increase in Ag doping concentration. 0.25% AgZnONPs had a bandgap energy of 3.69eV and that of 2.0% had a bandgap energy of 3.03eV. FT-IR spectra showed absorption in both functional group and fingerprint regions. The absorption band between 420- 470cm^{-1} is associated with that of the metal oxide. The PL spectrum showed emission at a wavelength of 350-500nm. The optical properties predict the possibility of using of Ag-ZnONPs in solar cells and optoelectronics.

***Corresponding author**

Joan Jepngetich, Department of Physical and Biological Sciences, Murang'a University of Technology, PO BOX 75, Murang'a 10200, Kenya.

Received: February 17, 2025; **Accepted:** February 24, 2025; **Published:** March 04, 2025

Keywords: Dopants, Bandgap, Nanoparticles, Ag-ZnONPs

Introduction

There is a significant development of inorganic nanoparticles in scientific field due to their wide application in electronics, medical field and information technology [1]. This can be supported by the growing number of scientific reports and companies working on scientific materials and nanotechnology, from which they are using inorganic nanoparticles for semiconductor technology as photocatalysts to conserve the environment [2].

Dye sensitized solar cells (DSSC), organic, perovskite and quantum dot are solar cell technologies that uses advanced and complex materials. Among the developed solar cell technologies, none has achieved the 90% theoretical energy conversion limit [3]. Bandgap energy is one of the major factors that affect the efficiency of any solar cell. This can be accounted for the fact that the incoming light must have enough energy to knock out electron. In scenarios where the light has more energy than the band gap, the extra energy is lost inform of heat. Consequently, if the light energy is less than the band gap it passes through it [4]. Nanostructured semiconductors such as ZnO have recently gained a great recognition in the solar cells industries due to their remarkable physical and chemical properties that differ from its bulk materials. ZnO is a semiconductor compound used in making the photoanode of solar cells due to its large band gap of 3.37eV and excitonic binding energy of 60 meV [5]. The impurity content, shape and size affect the optoelectronic behavior of nanostructured semiconductors and thus there is need for an in depth- understanding on fabrication of efficient materials. In the recent years, doping has been reported to influence the luminescence properties of ZnO. This has led to blueshift or redshift at near band edge (NBE) emission and in their visible emission [6]. Dopants like silver (Ag) are known to have a great impact on the luminescence properties of nanostructured semiconductors [7].

Various methods are used to prepare ZnONPs such as the wet chemical, hydrothermal method and precipitation [8-10]. However, these methods are considered to be harmful to the environment since they utilize toxic reagents and involve tedious procedure to prepare nanoparticles. Therefore, there is need to develop simple and green method to synthesize these nanoparticles. This method involves the use of plant extract as a capping and stabilizing agent to control the crystal growth of nanoparticles. Flavonoids, terpenoids, phenolics, aldehyde and ketones are the phytochemical components in plant extracts that act as reducing and stabilizing agents. *Citrus reticulata* (tangerine) which belongs to the Rutaceae family, contains abundant amount of polyphenols which are inexpensive, renewable and widely available and could be efficient for the growth of nanoparticles.

Phytochemical analysis of different parts of Citrus reticulate fruit revealed that the flavedo (outer peel) and albedo (white pith) have the highest concentration of phenolic contents than the juice sac [11]. The sum of phenolic contents in flavedo and albedo range from 22.02mg gallic acid equivalent (GAE) and 47.39mg dry weight [12].

This study report a low cost, facile, green and one pot method for synthesis of Ag-ZnONPs using *Citrus reticulata* peel extract without any additional reducing agent, acids or organic solvents. The effects of different Ag doping concentrations on the material properties of *Citrus reticulata* capped ZnONPs was studied in details to determine the optimum conditions for the growth of the AgZnONPs for photovoltaic applications.

Experimental Methods

Chemicals

All the chemicals used were of analytical grade and were used without any form of purification. Zinc acetate dihydrate ($Zn(CH_3COO)2.2H_2O$) (>98%), ammonia hydroxide(NH4OH)(>99%), silver nitrate($AgNO_3$) (>99.9%), ethanol (CH_3CH_2OH) (>99%) were purchased from Sigma Adrich & A.B Chem.Co,.Ltd. Deionized water was prepared in Murang'a University of Technology Research Laboratory.

Preparation of Citrus Reticulata Peel Extract

Citrus reticulata were purchased from the local market, washed with deionized water to remove surface pollutants, and hand peeled. To obtain the peel extract, the peels were dried in air in the absence of sunlight at temperature of about 27 - 28°C. The dried peels were then milled using an electric mill and sieve to powder. 50g of the sample was introduced to 500ml of deionized water and heated at temperature of 80°C for 15 minutes [13]. After cooling to ambient temperature, it was filtered with 1mm Whatman filter paper and stored in a refrigerator to be used as capping agent in the analysis.

Synthesis of Citrus Reticulata Capped Ag-ZnONPs

3.84g of zinc acetate dihydrate was dissolved in 50 ml of deionized water and stirred for 5 minutes at room temperature. 20 ml of *Citrus Reticulata* peel extract was added to the solution and stirred, after which 10 ml of ammonium hydroxide was added. Different concentration of silver nitrate (0.1, 0.25, 0.5, 0.75, 1.0, 1.5&2.0 mol %) were added and stirred at 40 °C for 3 hours. The nanoparticles formed were allowed to settle for 24 hours then washed with ethanol and dried in hot air oven for 2 hours at100 °C and annealed at 450 °C for 3 hours.

Characterization Technique

X-ray diffractometer (XRD) model ARL EQUINOX 100 was used at 40V, 0.9mA, at a scanning range of 2θ-100° and an interval time of 240 seconds to obtain the crystal structure and phase component of the synthesized ZnO nanoparticles. The data obtained was plotted in origin, analyzed and compared to those of standard in Joint committee on powder diffraction standards (JCPDS). Debye Scherrer equation was used to calculate the crystallite size of the nanoparticles formed. Fourier transform infrared spectroscopy (FT-IR) Shimadzu model was used to determine the functional groups present in the nanoparticles. Photoluminescence spectroscopy (PL) Infitek SPLF97 model was used to determine the electronic structure and defects in nanoparticles. Ultra violet visible spectroscopy evolution one plus model was used to determine the optical properties of nanoparticles.

Results and Discussion

X-ray Diffractions (XRD) Analysis

The XRD pattern for Ag-ZnO is shown in Figure 1 and it exclusively display the hexagonal wurtzite structure of ZnO which matches that of JCPDS file (no. 01-070-8072). The pattern depict only ZnO peaks. This means that successful doping was achieved with hydroxyl free *Citrus reticulata* peel extract. There was no peak patterns for Ag, all were incorporated to ZnO structure. They all occupied the interstitial site of the ZnO or were segregated into the nano crystalline region in the grain boundaries while conserving the original ZnO lattice structure [14]. The cell parameter (a) was calculated from peak (100) and c was calculated from peak (002) the results matches that obtained by Ranjithkumar et al [15].

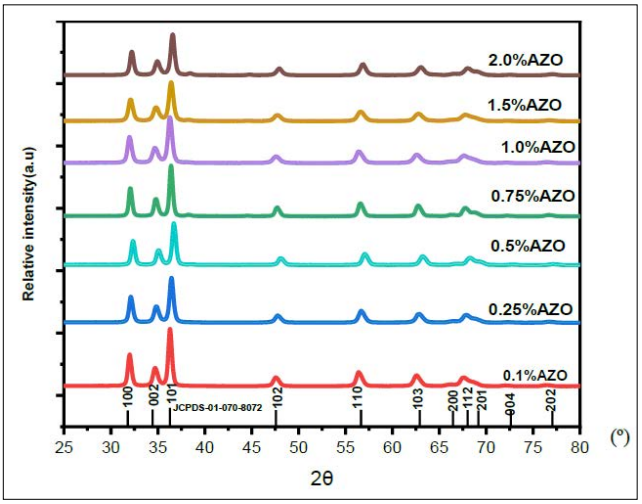

Figure 1: XRD Pattern for Ag-doped ZnONPs of 0.1, 0.25, 0.5, 0.75, 1.0, 1.5 and 2.0 mol%

The mean crystallite size and d spacing was calculated using the Debye-Scherrer formula and Bragg's equation respectively for the planes [100,002,101,102,110,103] and the results were summarized in Table 1 [16, 17].

The Bragg's equation is given by equation 1.

$$n\lambda = 2dsin\theta \qquad (1)$$

With λ being the wavelength, n is interger normally 1 and θ is the reflected angle, d is the crystal spacing. The Debye-Scherrer was used to calculate the crystal size of the Ag-ZnONPs. Crystal size characterization is important in determining the nature of particles as either small crystalline (soft), thermal behavior, diffusion and large crystalline which indicates hard materials [18].
The Scherrer equation is given by

$$D = \frac{K\lambda}{\beta COS\theta} \qquad (2)$$

Where D is the crystal size, K Scherrer constant (0.9), β denotes full width at half maximum for each plane peak and λ is the wavelength which was (1.5406Å) for Cu anode x-ray tube.

In Table 1 it was observed that the d-spacing increase when silver was introduced to ZnO structure. When dopants were added the d-spacing increased rapidly and on addition of higher mol % of silver dopant the spacing decrease gradually. The fluctuation in d-spacing can be associated to strain defect from varying the concentration of silver. The d- spacing at plane (002) decreases with increase in concentration of silver. The d-spacing effects were directly proportional to the effects encountered by lattice parameters. The c lattice parameter change from 5.192Å for undoped ZnO to 5.198Å when doped with 0.1% of silver. This indicates that doping increases the lattice parameters. When different concentrations were added, it was observed that the lattice parameters c decreases and the smallest value observed was for 0.75%. This stipulate that all the Ag ions had occupied the interstitial site of ZnONPs. The shift in peak position towards the higher 2 theta degree was also observed as the concentration of Ag was added. This

is in agreement with what Sampath et al observed when ZnO was doped with Ag prepared using Neem leaf extract, Hibiscus and Tulsi [19]. This factor is attributed to the fact that the Ag+ has larger ionic radius (0.126nm) compared to Zn+ (0.074nm).

Table 1: Effects of Different mol % Concentration of Silver Dopant on the d-spacing and Lattice Parameters a and c

Plane	100	002	101	102	110	103	Average d-spacing	a	c
2θ									
ZnO	31.52	34.52	36.17	47.48	56.36	62.49	2.129	3.084	5.192
0.1mol%Ag-ZnO	31.79	34.54	36.12	47.42	56.29	62.41	2.162	3.247	5.198
0.25mol%Ag-ZnO	31.10	34.72	36.33	42.67	56.59	62.73	2.191	3.318	5.163
0.5mol%Ag-ZnO	31.81	34.96	36.61	47.98	56.95	62.93	2.134	3.245	5.129
0.75mol%Ag-ZnO	31.93	34.67	36.29	47.60	56.51	62.65	2.142	3.233	5.129
1.0mol%Ag-ZnO	31.85	34.59	36.17	47.48	56.36	62.49	2.151	3.242	5.182
1.5mol%Ag-ZnO	31.92	34.66	36.27	47.49	56.49	62.63	2.147	3.235	5.172
2.0mol%Ag-ZnO	31.78	34.82	36.45	47.81	56.73	62.89	2.141	3.248	5.149

When the crystal size was calculated using Debye Scherrer formula (equation 2) it was noted that the size increased from 15.294 nm to 17.505 nm for 0.1% and the largest crystal size was found to be 19.867nm with 0.75% Ag dopant. The crystal size in peak (103) was small in all the samples with peak (100) having the largest crystal size. The crystal sizes were calculated from the average of the first three peaks [100], [002], and [101]. Table 2 shows the crystal size (D) and FWHM for AgZnONPs.

Table 2: Calculated Crystal Size (D) and obtained FWHM

Plane	100	002	101	102	110	103	D(nm)
FWHM							
ZnO	0.512282	0.59797	0.52914	0.75748	0.73448	0.87554	15.294
0.1mol%Ag-ZnO	0.43686	0.57062	0.43902	0.67911	0.66488	0.78343	17.505
0.25mol%Ag-ZnO	0.45721	0.58684	0.46139	0.69371	0.69204	0.80245	16.77
0.5mol%Ag-ZnO	0.43651	0.5378	0.45781	0.65871	0.67289	0.77519	17.562
0.75mol%Ag-ZnO	0.38866	0.47395	0.40253	0.56972	0.58283	0.65679	19.8672
1.0mol%Ag-ZnO	0.4947	0.6345	0.4903	0.79876	0.73629	0.89034	15.617
1.5mol%Ag-ZnO	0.52598	0.5920	0.52401	0.79177	0.79402	0.92176	15.239
2.0mol%Ag-ZnO	0.44006	0.54466	0.47248	0.67631	0.66495	0.77333	17.268

Figure 2 shows the variation in crystal size with FWHM for Ag-ZnO. From the pattern it was observed that the crystal size was inversely proportion to the FWHM: crystal size $\text{size} \propto \frac{1}{FWHM}$. When crystal size increased the FWHM decreased. These variation was not constant with variation in concentration with 0.75% dopant having the highest FWHM and lowest crystal size. The increase in crystal size is associated with decrease in strain. The sudden decrease in crystal size indicates that addition of silver dopant had reached its maximum level and could not occupy the interstitial sites of ZnO [20].

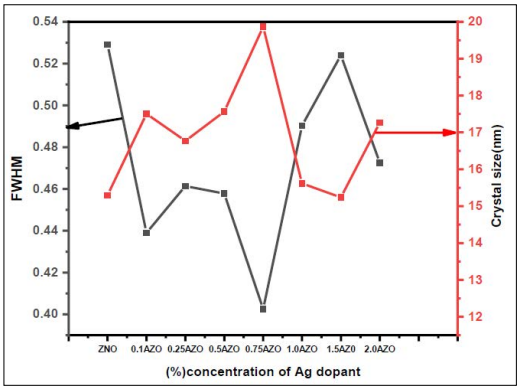

Figure 2: Variation of FWHM and Crystal Size of Pure ZnO, 0.1, 0.25, 0.5, 0.75, 1.0, 1.5 and 2.0 mol% Ag-ZnO Nanoparticles

Figure 3(a) shows the enlarged diffraction pattern of plane [101] at varying concentration of silver. The plane was used because it had the highest peak as compared to all the other mol% concentration of the dopant. From the pattern it can be observed that when 0.5% Ag was used the peak shift to the higher angle compared to other concentration of dopants. The highest peak observed was for 0.1% Ag this showed that the most crystalline particles were observed, when low concentration of silver was used. When the concentration of Ag was increased, the peak position shifted towards the lower values. The shift indicates partial substitution of Ag^{+} at the lattice sites of ZnO, which leads to an increase in lattice parameters a and c as expected but from the results obtained the c character decrease as the concentration of Ag was added until 0.75%. The c parameter started increasing then decreased this can be attributed to factors such as formation of silver nano-collection and strains depending on how the ZnO interacted with the dopant [21]. The peak intensity increased with a decrease in FWHM, this suggests that there is an improvement in crystallinity of nanoparticles [22]. 1.0% had slight effect from that of undoped ZnO, the intensity of the peak and FWHM were almost similar. In Figure 3(b) the variation of concentration with FWHM and relative intensity at plane 101 is displayed.

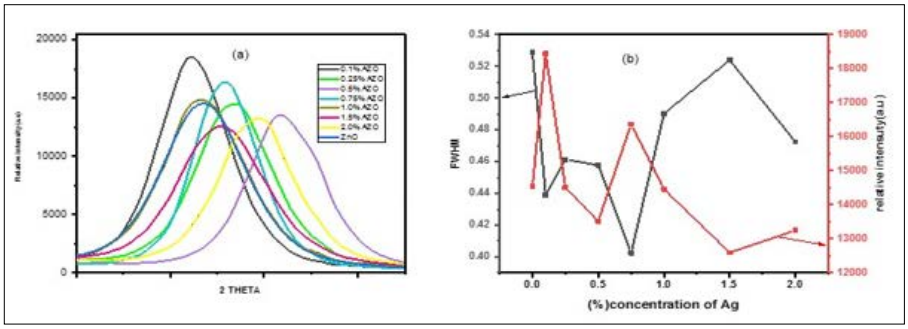

Figure 3: (a) Enlargement Image of Diffraction Plane [101] for Pure ZnO, 0.1, 0.25, 0.5, 0.75, 1.0, 1.5 and 2.0mol% Ag-ZnO. (b) Variation in FWHM and Relative Intensity of Peak [101] for pure ZnO and Various Concentration of Ag dopant.

Estimation of Strain

The Williamson-Hall method was used to calculate the strain. W-H plot was used to determine the crystal size. The broadening caused by crystallite was calculated using the Debye Scherrer equation.

$$\varepsilon = \frac{\beta_{hkl}}{4sin\theta} \qquad (3)$$

Where ϵ is the lattice strain, β is the FWHM of the XRD peak in radians, and θ is the Bragg angle. The strain induced due to crystal imperfection and distortion was calculated using equation (4) [23].

$$\varepsilon = \frac{\beta}{4tan\theta} \qquad (4)$$

Where ε the micro strain and β is is the FWHM. Equation (5) which is a Williamson-Hall equation was used to calculate the crystal size

$$\beta cos\theta = \varepsilon(4sin\theta) + \frac{K\lambda}{D} \qquad (5)$$

The equation above is a function of data which is equal to equation of a straight line given by

$$y = mx + c \qquad (6)$$

With c being the slope equal to $\frac{K\lambda}{D}$, y equal to $\beta cos\theta$ and ε is the slope. When a graph of $4sin\theta$ on the x-axis and $\beta cos\theta$ on the y-axis is plotted, the slope obtained showed the microstrain and the crystal size was calculated from the y-intercept. The strain obtained might have been a result of reduction of lattice parameters that was observed from the calculation of lattice parameters. Table 3 show the strain obtained by Williamson hall equation for different concentration of silver.

Table 3: Variation of Strain with Concentration from W-H Method

Ag (%)	Strain
0.1	0.00073236
0.25	0.00085902
0.5	0.00403
0.75	0.00348
1.0	0.01718
1.5	0.02881
2.0	0.00414

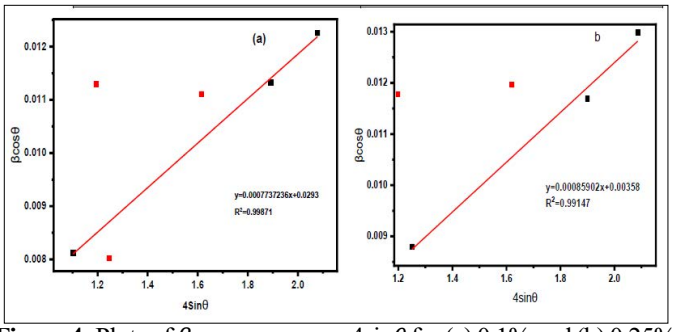

Figure 4: Plots of $\beta_{hklcos\theta}$ versus 4sinθ for (a) 0.1% and (b) 0.25% Ag-ZnO.

Figure 5 shows the variation of crystal size (D), strain and concentration. It can be observed that D was inversely proportional to strain. $D \propto \frac{1}{\varepsilon}$. The highest strain was at 1.5% and this can be associated with higher interaction of Ag and ZnO at higher concentration that leads to lattice mismatch and distortion of crystal structure. Nanoparticles with smaller crystal size have large surface area to volume ratio thus higher surface energy which caused higher strain. This leads to increase in crystal size with decrease in strain. In theory, if all the strain value agree, they form an angle of forty five degrees with x-axis and they all lie in a straight line [24]. The strain increased with the concentration of dopant and was inversely proportional to crystal size. 0.1% Ag-ZnO

had the smallest strain and 1.5% Ag-ZnO had the highest strain. This might be a result of increase in concentration of Ag caused stressed on the structure of ZnO thus higher strain with increase in concentration.

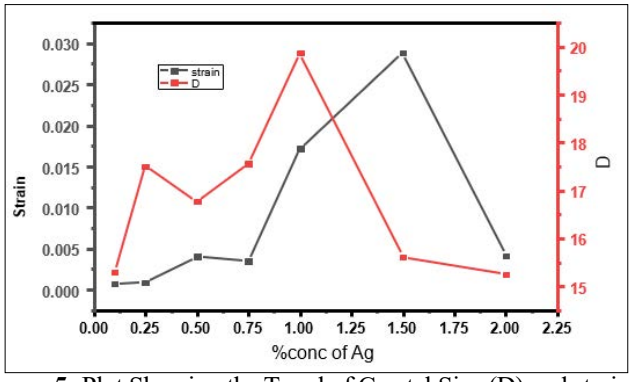

Figure 5: Plot Showing the Trend of Crystal Size (D) and strain of (0.1, 0.25, 0.5, 0.75, 1.0, 1.5 and 2.0 mol%) Ag-ZnONPs.

FT-IR Analysis of Different Concentration of Citrus Reticulata Capped Silver Dopant on ZnO Nanoparticles

From the pattern in Figure 6, the nanoparticles were absorbed in both the fingerprint region and the functional group region. The pattern gives the details on the functional groups present in the capping, stabilizing and reducing agents used to synthesize nanoparticles. The pattern obtained showed that O-H was in all prepared samples but when the samples were annealed; it was observed in 0.25, 0.5, 1.0 and 2.0 % Ag-ZnONPs only. This can be associated with the fact that at high temperature the OH group could have been vaporize with other water molecules. The presence of O-H group was shown by its absorption peak observed at the range of 2978-3633cm^{-1} in 0.25, 0.5, 0.75, 1.0, 1.5, and 2.0 % Ag. The O-H group of the annealed samples 0.25% Ag-ZnONPs had a very intense and more pronounce peak than in other dopant. The peaks becomes less intense when the concentration of silver decrease, this can be associated with partial substitution of silver ions in the ZnO lattice structure thus causing changes in the bond length [25]. Due to absorption of atmospheric CO_2 peaks were observed at 2968cm^{-1}. The low absorption mode at 1557cm^{-1} corresponds to C=C stretching modes. The elongated vibration at 1385cm^{-1} reveal the O-H bending frequency. At 1042cm^{-1} sharp peak was observed which corresponds to C-O whereas, the sharp stretching frequencies at 667 and 619cm- corresponds to C-H bending deformation vibration. The strong bands at 472 and 410cm- are attributed to the vibration elongation and deformation vibratory of Zn-O [26]. The as prepared samples spectrum shift to higher wave numbers as compared to annealed samples. 0.1% Ag-ZnO had the strongest vibration elongation of Zn-O for as prepared samples and 0.25% for annealed sample.

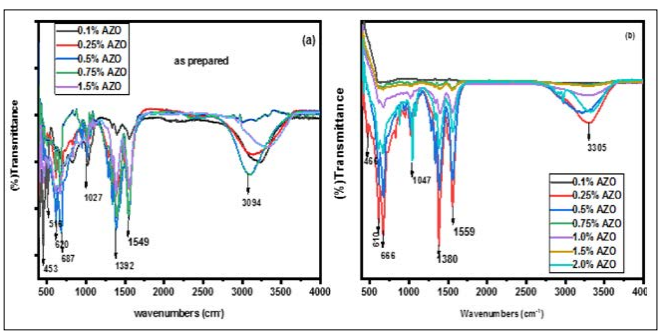

Figure 6: FT-IR Spectra of Annealed and as Prepared Samples

Photoluminescence Spectroscopy

Figure 7 shows the PL spectra of Ag-ZnONPs. ZnONPs were doped with different concentration of silver from 0.1, 0.25, 0.5, 0.75, 1.0, 1.5 and 2.0%. The samples were analyzed at room temperature at an excitation energy of 300nm. The study of photoluminescence of nanoparticles is important since it gives important details on the purity and quality of material synthesized. The PL spectra of ZnO nanoparticles analyzed at room temperature normally have two emission band: at the UV regions which is normally associated with near band edge emission through exciton-exciton collision process and at the visible region. The emission at the visible region is affiliated with electron hole recombination from the deep level emission (DLE) in the band gap caused by intrinsic and extrinsic defects [27]. The incorporation of hydroxyl group and carboxylates into the crystal structure during the growth of nanoparticles also contributes to visible region emissions [28]. The graph in Figure 7 showed that all the samples emit strongly in the UV region, with a band centered at 323nm which correspond to excitonic emission when excited at 300nm. The nanoparticle doped with 1.0% silver had the highest peak intensity and 2.0%Ag-ZnO nanoparticles had the lowest intensity. The emission spectra at 350-400nm was also observed. The sample with the highest intensity in the emission spectra was 1.5% Ag-ZnO nanoparticles and 0.25% had the lowest intensity.

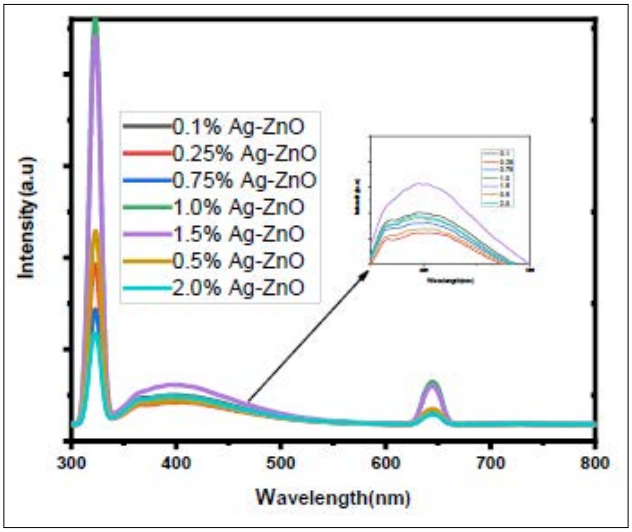

Figure 7: PL Emission Spectra of (0.1,0 .25, 0.5, 0.75, 1.0, 1.5 and 2.0 mol%) Ag-ZnO Nanoparticles

Burstein moss effect played a key role in shifting the PL emission spectra of Ag-ZnO nanoparticles to the UV region [29]. When ZnO is doped with metal, the Fermi level shift to the conduction band CB. It can be confirmed that the transition moved from the valence band (VB) to the conduction band (CB) in the Fermi level instead of from VB to the bottom of CB [30]. These changes in the transitions leads to band gap broadening thus blue shift. The blue shift emission in the UV regions changes with doping concentration. In figure 8 it was observed that increased in Ag concentration shift the emission to a higher wavelength with 364, 365, 364, 366, 368 and 370 for 0.1, 0.25, 0.5, 0.75, 1.0, 1.0 and 2.0% Ag-ZnONPs. This results were also observed by Ungula *et.al* [31].

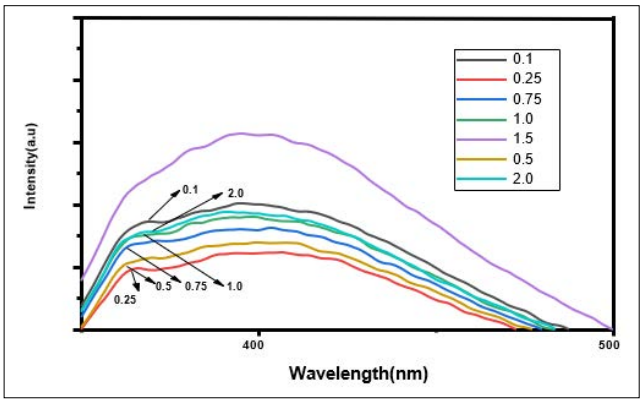

Figure 8: Room Temperature PL Emission Spectra of 0.1, 0.25, 0.5, 0.75, 1.0, 1.5 and 2.0 mol% AgZnONPs.

Optical Properties

The absorption spectra of pure ZnO and silver doped ZnONPs is shown in Figure 9. The analysis was carried out at room temperature in the wavelength range of 200-800nm. Strong absorption edge in the region between 200-400nm (UV region) was observed. The absorption occurred as a result of charge transfer from the valence band (VB) to conduction band (CB) [32]. The absorption increased with an increase in concentration of silver dopant. This change in the absorption peak with concentration of dopants confirms the change in the energy gap [33]. The weak absorption start from 500 and maximum absorptions are observed between 280-400nm.

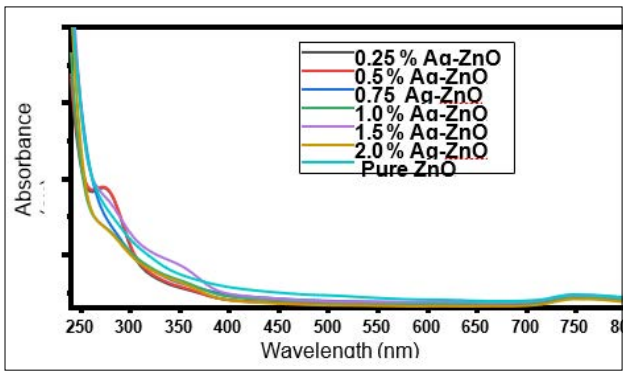

Figure 9: UV-vis spectra of pure, 0.25, 0.5, 0.75, 1.0, 1.5 and 2.0% Ag-ZnONPs

The band gap energy was obtained by plotting a graph of $(\alpha hv)^2$ versus energy (eV) then extrapolated according to Tauc's equation (7)

$$(\alpha hv)^{\gamma}=A(hv-Eg) \qquad (7)$$

Where Eg is the bandgap energy, A is a constant, h is the plank's constant, v is the photon frequency, α symbolize absorption coefficient and γ designate the electronic transition and can be 2 or ½ for direct and indirect allowed transition respectively. It can also denote direct or indirect forbidden transition if its 2/3 and 1/3 respectively. If Taucs equation is compared to the equation of straight such that

$$Y = m(x) \qquad (8)$$

Putting the y axis equal to zero then

$$0=A(hv-Eg) \qquad (9)$$

Thus hv = Eg

Figure 10 shows the bandgap energies of different concentration of Silver dopant in ZnONPs. The band gap energies decrease with an increase in silver concentration from 3.69, 3.61, 3.17, 3.10, 3.13, 3.03 and 3.30 eV for 0.25%, 0.5%, 0.75%, 1.0%, 1.5%, 2.0% and pure ZnO respectively. ZnO bandgap widen when doped with donors but decreased when doped with acceptors. The bandgap energy increases slightly when doped with lower percentage of Ag due to quantum effect. When the concentration of dopant is increased it weaken the confinement effects by increasing the defects level thus decrease in bandgap [34].

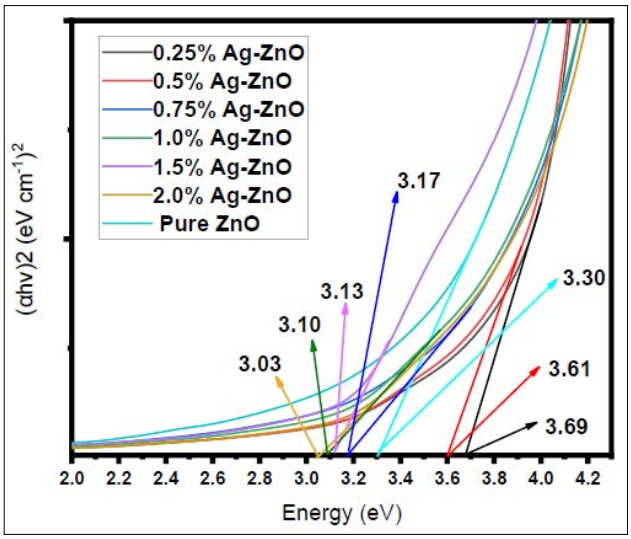

Figure 10: Tauc's Plot Showing Estimated Bandgap Energies of Pure, 0.25, 0.5, 0.75, 1.0, 1.5 and 2.0 mol% Ag-ZnONPs.

Conclusion

In summary, the structural, optical and morphological properties of ZnONPs were influenced by the amount of silver dopant added. XRD analysis confirmed that the hexagonal wurtzite structure of ZnO was maintained when silver was added. The crystal size was inversely proportional to FWHM. The FT-IR absorption at fingerprint region 470-420 confirmed the presence of metal oxide bond. The PL spectra confirmed that Fermini effect was observed when Ag was added to ZnONPs. The emission band shift to a higher emission wavelength with increase in dopant concentration. The bandgap energies of nanoparticles decrease with increase in Ag concentration. This study suggest that Ag dopant controlled the luminescence properties and produced p type of conductivity.

Acknowledgments

This publication was possible thanks to the SG-NAPI ward supported by the German Ministry of Education and Research, BMBF through UNESCO-TWAS. The authors also wished to thank Murang'a University of Technology for providing us with synthesis and characterization equipment.

Conflict of Interest

None

References

1. Mohagheghpour E, Moztarzadeh F, Rabiee M, Tahriri M, Ashuri M, et al. (2012) Micro-Emulsion Synthesis, Surface Modification, and Photophysical Properties of Zn, Mn &S Nanocrystals for Biomolecular Recognition. IEEE transactions on nanobioscience 11: 317-323.
2. Pham TAT, Tran VA, Le VD, Nguyen MV, Truong DD, et al. (2020) Facile preparation of ZnO nanoparticles and Ag/ZnO nanocomposite and their photocatalytic activities under visible

light. International Journal of Photoenergy 8897667.
3. Wibowo A, Marsudi MA, Amal MI, Ananda MB, Stephanie R, et al. (2020) ZnO nanostructured materials for emerging solar cell applications. RSC Advances 10: 42838-42859.
4. Sethi VK, Pandey M, Shukla MP (2011) Use of nanotechnology in solar PV cell. International Journal of Chemical Engineering and Applications 2: 77.
5. Sáenz Trevizo A, Amézaga Madrid P, Pizá-Ruiz P, Antúnez-Flores W, MikiYoshida M (2016) Optical band gap estimation of ZnO nanorods. Materials Research 19: 33-38.
6. Wang JTW, Wang Z, Pathak S, Zhang W, deQuilettes DW, et al. (2016) Efficient perovskite solar cells by metal ion doping. Energy & Environmental Science 9: 2892-2901.
7. Hosseini SM, Sarsari IA, Kameli P, Salamati H (2015) Effect of Ag doping on structural, optical, and photocatalytic properties of ZnO nanoparticles. Journal of Alloys and Compounds 640: 408-415.
8. Dien ND (2019) Preparation of various morphologies of ZnO nanostructure through wet chemical methods. Adv Mater Sci 4: 1-5.
9. Gerbreders V, Krasovska M, Sledevskis E, Gerbreders A, Mihailova I, et al. (2020) Hydrothermal synthesis of ZnO nanostructures with controllable morphology change. Cryst Eng Comm 22: 1346-1358.
10. Ghorbani HR, Mehr FP, Pazoki H, Rahmani BM (2015) Synthesis of ZnO nanoparticles by precipitation method. Orient J Chem 31: 1219-1221.
11. Wang Y, Qian J, Cao J, Wang D, Liu C, et al. (2017) Antioxidant capacity, anticancer ability and flavonoids composition of 35 citrus (Citrus reticulata Blanco) varieties. Molecules 22: 1114.
12. Zhang Y, Sun Y, Xi W, Shen Y, Qiao L, et al. (2014) Phenolic compositions and antioxidant capacities of Chinese wild mandarin (Citrus reticulata Blanco) fruits. Food chemistry 145: 674-680.
13. Ehrampoush MH, Miria M, Salmani MH, Mahvi AH (2015) Cadmium removal from aqueous solution by green synthesis iron oxide nanoparticles with tangerine peel extract. Journal of Environmental Health Science and Engineering 13: 17.
14. Ko YD, Kim KC, Kim YS (2012) Effects of substrate temperature on the Gadoped ZnO films as an anode material of organic light emitting diodes. Superlattices and Microstructures 51: 933-941.
15. Ranjithkumar B, Kumar ER, Srinivas M, Ramalingam HB, Srinivas C, et al. (2021) Evaluation of structural, surface morphological and thermal properties of Ag-doped ZnO nanoparticles for antimicrobial activities. Physica E: Low-dimensional Systems and Nanostructures 133: 114801.
16. Bett K, Kiprotich S (2024) Effects of Stirring Speed of Precursor Solution on the Structural Optical and Morphological Properties of ZnO Al Ga CoDoped Nanoparticles Synthesized via a Facile Sol Gel Technique. American Journal of Condensed Matter Physics 13: 9-20.
17. Abdulrahman NA, Haddad NI (2020) Braggs, Scherre, Williamson–Hall and SSP analyses to estimate the variation of crystallites sizes and lattice constants for ZnO nanoparticles synthesized at different temperatures. Neuro Quantology 18: 53.
18. Akbari B, Tavandashti MP, Zandrahimi M (2011) Particle size characterization of nanoparticles–a practical approach. Iranian Journal of Materials Science and Engineering 8: 48-56.
19. Sampath S, Bhushan M, Saxena V, Pandey LM, Singh LR (2022) Green synthesis of Ag doped ZnO nanoparticles: Study of their structural, optical, thermal and antibacterial properties. Materials Technology 37: 2785-2794.
20. Amit Y, Li Y, Frenkel AI, Banin U (2015) From impurity doping to metallic growth in diffusion doping: properties and structure of silver-doped InAs nanocrystals. ACS nano 9: 10790-10800.
21. Hosseini SM, Sarsari IA, Kameli P, Salamati Hjj (2015) Effect of Ag doping on structural, optical, and photocatalytic properties of ZnO nanoparticles. Journal of Alloys and Compounds 640: 408-415.
22. Ungula J (2018) Formation and characterization of novel nanostructured un-doped and Ga-doped ZnO transparent conducting thin films for photoelectrode [PhD Thesis, University of the Free State (Qwaqwa Campus)] https://www.academia.edu/103461558/Formation_and_characterization_of_novel_nanostructured_un_doped_and_Ga_doped_ZnO_transparent_conducting_thin_films_for_photoelectrode.
23. Bindu P, Thomas S (2014) Estimation of lattice strain in ZnO nanoparticles: X-ray peak profile analysis. Journal of Theoretical and Applied Physics 8: 123-134.
24. Aly KA, Khalil NM, Algamal Y, Saleem QM (2016) Lattice strain estimation for CoAl2O4 nano particles using Williamson-Hall analysis. Journal of Alloys and Compounds 676: 606-612.
25. Murtaza G, Ahmad R, Rashid MS, Hassan M, Hussnain A, et al. (2014) Structural and magnetic studies on Zr doped ZnO diluted magnetic semiconductor. Current Applied Physics 14: 176-181.
26. Sorbiun M, Shayegan Mehr E, Ramazani A, Taghavi Fardood S (2018) Biosynthesis of Ag, ZnO and bimetallic Ag/ZnO alloy nanoparticles by aqueous extract of oak fruit hull (Jaft) and investigation of photocatalytic activity of ZnO and bimetallic Ag/ZnO for degradation of basic violet 3 dye. Journal of Materials Science: Materials in Electronics 29: 2806-2814.
27. Bandopadhyay K, Mitra J (2015) Zn interstitials and O vacancies responsible for ntype ZnO: what do the emission spectra reveal?. Rsc Advances 5: 23540-23547.
28. Kozak O, Sudolska M, Pramanik G, Cigler P, Otyepka M, et al. (2016) Photoluminescent carbon nanostructures. Chemistry of Materials 28: 4085-4128.
29. Campbell B, Kelly P, Talamantes A, Kuznetsova L (2020) The interplay between bandgap renormalization and Burstein-Moss effect for multilayered Al: ZnO/ZnO metamaterial. In Metamaterials, Metadevices, and Metasystems 11460: 114600H
30. Saw KG, Aznan NM, Yam FK, Ng SS, Pung SY (2015) New insights on the burstein-moss shift and band gap narrowing in indium-doped zinc oxide thin films. PloS one 10: e0141180.
31. Ungula J, Kiprotich S, Swart HC, Dejene BF (2022) Investigation on the material properties of ZnO nanorods deposited on Ga-doped ZnO seeded glass substrate: Effects of CBD precursor concentration. Surface and Interface Analysis 54: 10231031.
32. Wagh SS, Jagtap CV, Kadam VS, Shaikh SF, Ubaidullah M, et al. (2022) Silver doped ZnO nanoparticles synthesized for photocatalysis application. ES Energy & Environment 17: 94-105.
33. Hosseini SM, Sarsari IA, Kameli P, Salamati H (2015) Effect of Ag doping on structural, optical, and photocatalytic properties of ZnO nanoparticles. Journal of Alloys and Compounds 640: 408-415.
34. Amrute V, Supin KK, Vasundhara M, Chanda A (2024) Observation of excellent photocatalytic and antibacterial activity of Ag doped ZnO nanoparticles. RSC advances 14: 32786-32801.

Copyright: ©2025 Joan Jepngetich, et al. This is an open-access article distributed under the terms of the Creative Commons Attribution License, which permits unrestricted use, distribution, and reproduction in any medium, provided the original author and source are edited.